3-D Path-Following Control for a Model-Scaled Autonomous Helicopter

Bing Zhu, *Member, IEEE*, and Wei Huo, *Member, IEEE*

***Abstract*— A 3-D path-following controller is proposed in this brief for a 6-degrees-of-freedom model-scaled autonomous helicopter. The reference path and path-following errors are newly defined using implicit expressions. On the basis of geometric analysis, a new speed error is designed for singularity avoidance. The proposed control algorithm is designed using command filtered backstepping, such that complicated solutions for derivatives of virtual controls are circumvented. It is proved that, with the proposed controller, path-following errors are locally ultimately bounded. Theoretical results are demonstrated by the numerical simulation.**

***Index Terms*— Command filtered backstepping, nonlinear control, path-following, singularity avoidance, unmanned helicopter.**

I. Introduction

REFERENCE tracking problems for mechanical systems can be roughly divided into three categories: 1) point stabilization; 2) trajectory tracking; and 3) path-following. In the first two categories, closed-loop systems are expected to track reference points or time-based reference trajectories. Path-following differs from trajectory tracking in that no specific temporal requirements are assigned for the controlled vehicles and reference paths. It has been claimed during recent years that path-following controllers are more applicable than trajectory-tracking controllers in some specific areas [1].

Some recent representative theoretical researches on path-following control of nonlinear systems can be referred to [2], [3], where path-following controllers are designed for nonlinear systems with unstable zero dynamics. Path-following problems are also studied extensively for control of planar or 3-D moving vehicles (e.g., wheeled robots [4], underwater vehicles [5], fixed-wing aerial vehicles [6], [7], and snake-like robot [8]).

Parameterized path-following is the most prevalent formulation of the problem. The reference path is given by a parameterized curve, and the task is to design an updating law for the path parameter [3], [5], [9], so that the path-following problem becomes a point-tracking problem. Updating law for the path parameter can be regarded as an extra control input that excludes performance limitations imposed on trajectory tracking [1]. Moreover, using parameterized path-following control, control singularities can be avoided effectively [6]. However, there exist some drawbacks in parameterized path-following control. For specific analysis, please see [10].

Another solution to the path-following problem is to design a controller to stabilize path-following errors defined by implicit expressions. For 2-D (planar) path-following, the reference path is given by a 2-D manifold; while for 3-D path-following, the reference path is given by intersecting two 3-D manifolds [10]. With this approach, the controlled vehicle would enter into an invariant set enclosing the reference path. The objective is to follow the entire reference path instead of any moving points. However, path-following control based on implicit reference path often suffers from singularities; thus, its potential applications are greatly impeded.

In this brief, a new 3-D path-following controller for a 6-degrees-of-freedom (DOF) model-scaled helicopter is proposed to overcome the drawback of singularities. The reference path to be followed is given by intersecting two 3-D manifolds. Local singularities around the reference path are avoided using the new definition of speed error. The path-following controller is designed with a newly developed technique named command filtered backstepping [11], [12]. It is proved that, with the proposed controller, path-following errors are locally ultimately bounded. Simulation results are presented to demonstrate the theoretical results. Main contributions of this brief include: 1) the new formulation of the 3-D path-following errors and the speed error; 2) the strategy of singularity avoidance based on geometric analysis; and 3) the application of command filtered backstepping to circumvent complicated solutions for derivatives of virtual controls.

This brief is organized as follows. The path-following problem is formulated in Section II; detailed procedures of controller design are described in Section III; the simulation results are shown in Section IV; and conclusion and future works are presented in Section V.

II. Problem Statement

A. Notations

In this brief, the notation $|\cdot|$ denotes absolute value for real numbers, and the notation $\|\cdot\|$ denotes Euclidean norm or induced Euclidean norm for vectors (covectors) or matrices, respectively.

Manuscript received November 21, 2012; revised May 3, 2013 and September 7, 2013; accepted December 17, 2013. Manuscript received in final form December 21, 2013. Date of publication January 4, 2014; date of current version July 24, 2014. This work was supported by the National Natural Science Foundation of China under Grant 61074010. Recommended by Associate Editor N. Hovakimyan.

B. Zhu was with the Seventh Research Division, and Science and Technology on Aircraft Control Laboratory, Beihang University, Beijing 100191, China. He is now with the Department of Electrical, Electronic and Computer Engineering, University of Pretoria, Pretoria 0002, South Africa (e-mail: bing.zhu@up.ac.za).

W. Huo is with the Seventh Research Division, and Science and Technology on Aircraft Control Laboratory, Beihang University, Beijing 100191, China (e-mail: weihuo@buaa.edu.cn).

Color versions of one or more of the figures in this paper are available online at http://ieeexplore.ieee.org.

Digital Object Identifier 10.1109/TCST.2013.2296519

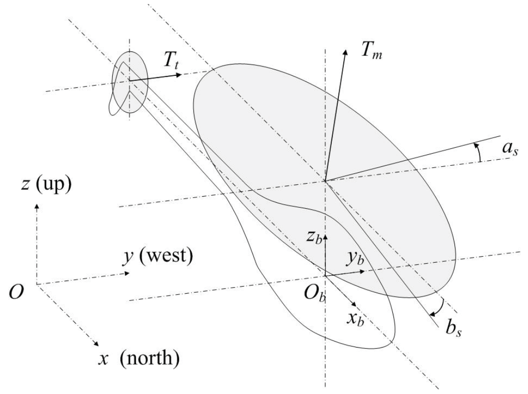

Fig. 1. Simple illustration of the helicopter model, including reference frames, flapping angles, and thrusts generated by rotors.

For any continuously differentiable vector function $F(x) = [f_1(x), \ldots, f_m(x)]^T : \mathbb{R}^n \to \mathbb{R}^m$, where $x = [x_1, \ldots, x_n]^T \in \mathbb{R}^n$, its Jacobian matrix is defined by

$$\frac{\partial F}{\partial x} \triangleq \begin{bmatrix} \frac{\partial f_1}{\partial x_1} & \cdots & \frac{\partial f_1}{\partial x_n} \\ \vdots & \ddots & \vdots \\ \frac{\partial f_m}{\partial x_1} & \cdots & \frac{\partial f_m}{\partial x_n} \end{bmatrix}.$$

The cross product of covectors (row vectors) is defined by $x^T \times y^T \triangleq (x \times y)^T$, where x and y are vectors, and the cross product of vectors $x \times y$ is defined conventionally.

B. Mathematical Modeling for Model-Scaled Helicopter

The helicopter model is shown in Fig. 1. For mathematical modeling, we use two traditional reference frames: 1) the earth reference frame (ERF) and 2) the fuselage reference frame (FRF). For detailed definitions, please see [13].

The mathematical model of the model-scaled unmanned helicopter could be derived by Newton–Euler equations [14], [15]

$$\dot{P} = V \tag{1}$$

$$m\dot{V} = -mg_3 + R(\gamma)F \tag{2}$$

$$\dot{R}(\gamma) = R(\gamma)S(\omega) \tag{3}$$

$$J\dot{\omega} = -S(\omega)J\omega + Q \tag{4}$$

where $P \triangleq [x, y, z]^T$ and $V \triangleq [u, v, w]^T$ are position and velocity of c.g. of the helicopter in ERF, respectively, m denotes the mass, $g_3 \triangleq [0, 0, g]^T$ and g is the gravitational acceleration, $\gamma \triangleq [\phi, \theta, \psi]^T$ denotes the attitude in ERF, and the rotational matrix is given by

$$R = [R_{ij}] \triangleq \begin{bmatrix} \mathrm{c}\theta\mathrm{c}\psi & \mathrm{c}\psi\mathrm{s}\theta\mathrm{s}\phi - \mathrm{c}\phi\mathrm{s}\psi & \mathrm{c}\phi\mathrm{c}\psi\mathrm{s}\theta + \mathrm{s}\phi\mathrm{s}\psi \\ \mathrm{c}\theta\mathrm{s}\psi & \mathrm{s}\psi\mathrm{s}\theta\mathrm{s}\phi + \mathrm{c}\phi\mathrm{c}\psi & \mathrm{c}\phi\mathrm{s}\psi\mathrm{s}\theta - \mathrm{s}\phi\mathrm{c}\psi \\ -\mathrm{s}\theta & \mathrm{c}\theta\mathrm{s}\phi & \mathrm{c}\theta\mathrm{c}\phi \end{bmatrix}$$

where $\mathrm{c}(\cdot)$ and $\mathrm{s}(\cdot)$ are the shorts for $\cos(\cdot)$ and $\sin(\cdot)$, respectively, $\omega \triangleq [p, q, r]^T$ represents the angular velocity in FRF, and $S(\cdot)$ denotes the skew-symmetric matrix such that $S(\omega)J\omega = \omega \times J\omega$; the inertial matrix is given by

$$J \triangleq \begin{bmatrix} I_{xx} & 0 & -I_{xz} \\ 0 & I_{yy} & 0 \\ -I_{xz} & 0 & I_{zz} \end{bmatrix}.$$

Resultant forces and torques in FRF are given by

$$F = \begin{bmatrix} T_m \mathrm{s}a_s \\ -T_m \mathrm{s}b_s + T_t \\ T_m \mathrm{c}b_s \mathrm{c}a_s \end{bmatrix} \tag{5}$$

$$Q = \begin{bmatrix} T_m h_m \mathrm{s}b_s + L_b b_s + T_t h_t + Q_m \mathrm{s}a_s \\ T_m l_m + T_m h_m \mathrm{s}a_s + M_a a_s + Q_t - Q_m \mathrm{s}b_s \\ -T_m l_m \mathrm{s}b_s - T_t l_t + Q_m \mathrm{c}a_s \mathrm{c}b_s \end{bmatrix} \tag{6}$$

where T_m, Q_m, T_t, and Q_t represent the thrusts and the counteractive torques generated by the main rotor and the tail rotor, respectively; h_m, h_t, l_m, and l_t are the vertical and horizontal distances between the c.g. of the helicopter and the centers of the rotors, respectively; L_b and M_a are longitudinal and lateral stiffness coefficients of main rotor blades; and a_s and b_s are the longitudinal and lateral flapping angles, respectively. Since it is extremely fast compared with the fuselage dynamics, the flapping dynamics can be neglected in this brief. Expressions for thrusts with respect to collective pitches are given by [16]

$$T_i = t_{ci}\rho s_i A_i \Omega_i^2 R_i^2 \tag{7}$$

$$t_{ci} = \frac{1}{4}\left[-\frac{a_i}{4}\sqrt{\frac{s_i}{2}} + \sqrt{\frac{a_i^2 s_i}{32} + \frac{2}{3}a_i\theta_i}\right]^2 \tag{8}$$

and expressions for counteractive torques are given by

$$Q_i = q_{ci}\rho s_i A_i \Omega_i^2 R_i^3, \quad q_{ci} = \frac{\delta_d}{8} + 1.13 t_{ci}^{\frac{3}{2}}\sqrt{\frac{s_i}{2}} \tag{9}$$

where subscripts ($i = m, t$) represent the main and tail rotors, respectively; θ_i denotes the collective pitch of the main or tail rotor; ρ, s_i, a_i, A_i, Ω_i, and R_i denote the density of air, the solidity of the rotor disk, the slope of the lift curve, the area of the rotor disc, the rotational rate of rotors, and the radius of the rotor disc, respectively; and δ_d is the drag coefficient with a typical value of 0.012 [16]. Motion of the helicopter is controlled by θ_m, θ_t, a_s, and b_s.

C. Control Objective

The reference path to be followed is a regular curve described by implicit expression

$$\mathscr{P}_r = \left\{[x_r, y_r, z_r]^T \in \mathbb{R}^3 \,\middle|\, f_1(x_r, y_r, z_r) = 0,\ f_2(x_r, y_r, z_r) = 0\right\} \tag{10}$$

where $f_1(x, y, z)$ and $f_2(x, y, z)$ are C^∞ functions with respect to x, y, and z. The tangent covector of the reference path satisfies

$$\left.\frac{\partial f_1}{\partial P} \times \frac{\partial f_2}{\partial P}\right|_{P = P_r} \neq 0 \tag{11}$$

where $P_r \in \mathscr{P}_r$.

Remark 1: Physically, $\partial f_1/\partial P$ and $\partial f_2/\partial P$ are normal covectors of manifolds $f_1 = 0$ and $f_2 = 0$, respectively, and the cross product $\partial f_1/\partial P \times \partial f_2/\partial P|_{P=P_r}$ denotes the tangent covector of the reference path. On a regular curve, $\partial f_1/\partial P$ and $\partial f_2/\partial P$ are unparallel, and the tangent covector is nonzero. Furthermore, the C^∞ property of f_1 and f_2 implies that $\partial f_1/\partial P \times \partial f_2/\partial P$ is C^∞, then it holds that $\partial f_1/\partial P \times \partial f_2/\partial P \neq 0$ in the near region of the reference path.

The objective of this brief is to design a path-following controller, such that the controlled helicopter follows the reference path (10) with a reference speed $v_r > 0$, or mathematically

$$\begin{cases} \lim_{t\to\infty} \ |f_1(x(t), y(t), z(t))| < \bar{\varepsilon}_1 \\ \lim_{t\to\infty} \ |f_2(x(t), y(t), z(t))| < \bar{\varepsilon}_2 \\ \lim_{t\to\infty} \ |\|V(t)\| - v_r| < \bar{\varepsilon}_3 \end{cases} \tag{12}$$

where $\bar{\varepsilon}_1$, $\bar{\varepsilon}_2$, and $\bar{\varepsilon}_3$ are small positive numbers.

Remark 2: Reference path given by (10) is an intersection of two 3-D manifolds (e.g., the reference path given in Section IV is an intersection of a ball and a plane). Physical implication of the first two equations in (12) is that if the actual position of the controlled vehicle approaches both manifolds, then it approaches the reference path. The third equation in (12) implies that actual speed approaches the reference speed.

III. Path-Following Controller Design

In this section, detailed controller design procedures for the model-scaled helicopter are presented. The helicopter model is simplified into a feedforward form to facilitate backstepping design. Path-following errors are defined based on implicit expressions, and are stabilized by virtual control without singularities. Control thrust T_m and control torque Q are designed according to command filtered backstepping [11], [12]. Actual controls θ_m, θ_t, a_s, and b_s are solved from T_m and Q.

A. Model Simplification and Transformation

The helicopter model (1)–(4) is strongly coupled, and it should be simplified and transformed to facilitate controller design. Since the cyclic flapping angles and the tail rotor thrust are fairly small according to the physical properties of the helicopter [15], [17], [18], it is reasonable to take $F = [0, 0, T_m]^T$ in (5) for simplification, and it follows that:

$$m\dot{V} = -mg_3 + R_3(\gamma)T_m \tag{13}$$

where R_3 denotes the third column of R. Approximating (2) with (13) enables the helicopter model to appear cascaded, and facilitates backstepping design.

Furthermore, the attitude kinematics can be described by

$$\dot{R}_3 = \dot{R}e_3 = \mathrm{RS}(\omega)e_3 = -\mathrm{RS}(e_3)\omega \tag{14}$$

where $e_3 \triangleq [0, 0, 1]^T$, $\|R_3\| = 1$, and R_{33} depends completely on R_{13} and R_{23}. Extracting the first two lines of (14) yields

$$\dot{\bar{R}}_3 = \begin{bmatrix} \dot{R}_{13} \\ \dot{R}_{23} \end{bmatrix} = \begin{bmatrix} -R_{12} & R_{11} \\ -R_{22} & R_{21} \end{bmatrix} \begin{bmatrix} p \\ q \end{bmatrix} = \hat{R}\bar{\omega} \tag{15}$$

where $\bar{R}_3 \triangleq [R_{13}, R_{23}]^T$, $\bar{\omega} \triangleq [p, q]^T$. The yaw kinematics can be given by [14]

$$\dot{\psi} = \frac{\mathrm{s}\phi}{\mathrm{c}\theta}q + \frac{\mathrm{c}\phi}{\mathrm{c}\theta}r. \tag{16}$$

Defining $\gamma_R \triangleq [\bar{R}_3^T, \psi]^T$, it can be proved that $\det(\partial\gamma_R/\partial\gamma) = \cos\theta > 0$ in the case of $|\theta| < \pi/2$. Therefore, the map from γ to γ_R is a local topological homeomorphism according to the inverse function theorem, suggesting that (15) and (16) are capable of representing the attitude kinematics under $|\theta| < \pi/2$. $|\theta| \geq \pi/2$ implies an uncontrollable situation, where gravity of the fuselage cannot be addressed by the main rotor.

Assumption 1: Roll and pitch of the helicopter fuselage satisfy $|\phi| < \pi/2$ and $|\theta| < \pi/2$.

The counteractive torque of the tail rotor Q_t contributes a tiny part of M, and is also negligible; therefore, the torques in (6) can be simplified by

$$Q = Q_A\tau + Q_B \tag{17}$$

where

$$Q_A = \begin{bmatrix} h_t & Q_m & T_m h_m + L_b \\ 0 & T_m h_m + M_a & -Q_m \\ -l_t & 0 & -T_m l_m \end{bmatrix}, \quad Q_B = \begin{bmatrix} 0 \\ T_m l_m \\ Q_m \end{bmatrix}$$

and $\tau \triangleq [T_t, a_s, b_s]^T$. Simplification of torques facilitates calculating the actual controls.

In summary, the simplified helicopter model can be expressed by (1), (4), (13), and (15)–(17).

B. Singularity Avoidance

In this brief, we consider the path-following errors

$$\begin{cases} \varepsilon_1 \triangleq f_1(x(t), y(t), z(t)) \\ \varepsilon_2 \triangleq f_2(x(t), y(t), z(t)). \end{cases} \tag{18}$$

It follows that:

$$\begin{cases} \dot{\varepsilon}_1 = \frac{\partial f_1}{\partial P} \quad \dot{P} = \frac{\partial f_1}{\partial P}V \\ \dot{\varepsilon}_2 = \frac{\partial f_2}{\partial P} \quad \dot{P} = \frac{\partial f_2}{\partial P}V \end{cases}, \quad \begin{cases} \ddot{\varepsilon}_1 = H_1 + G_1\dot{V} \\ \ddot{\varepsilon}_2 = H_2 + G_2\dot{V} \end{cases} \tag{19}$$

where, for $i = 1, 2$

$$\begin{aligned} H_i &= \frac{\partial^2 f_i}{\partial x^2}\dot{x}^2 + \frac{\partial^2 f_i}{\partial y^2}\dot{y}^2 + \frac{\partial^2 f_i}{\partial z^2}\dot{z}^2 + 2\frac{\partial^2 f_i}{\partial x\partial y}\dot{x}\dot{y} \\ &\quad + 2\frac{\partial^2 f_i}{\partial y\partial z}\dot{y}\dot{z} + 2\frac{\partial^2 f_i}{\partial z\partial x}\dot{z}\dot{x} \\ G_i &= \frac{\partial f_i}{\partial P}. \end{aligned}$$

Remark 3: Typically, the speed error is defined by

$$\varepsilon_3 \triangleq (V^T V - v_r^2)/2 \tag{20}$$

such that $\dot{\varepsilon}_3 = V^T\dot{V} - v_r\dot{v}_r$. Then

$$[\ddot{\varepsilon}_1 \ \ \ddot{\varepsilon}_2 \ \ \dot{\varepsilon}_3]^T = H + G\dot{V} = H + G\left(-g_3 + \frac{R_3 T_m}{m}\right) \tag{21}$$

where $H = [H_1, H_2, -v_r\dot{v}_r]^T$ and $G = [G_1^T, G_2^T, V]^T$. As can be observed, control thrust and attitude appear in (21).

Remark 4: It is obvious that singularities would occur when $\det(G) = (\partial f_1/\partial P \times \partial f_2/\partial P)\,V = 0$. Physically, singularities result from the following reasons:

- S1 the actual speed $\|V\| = 0$;
- S2 the actual velocity V is perpendicular to tangent covector of the desired path: $(\partial f_1/\partial P \times \partial f_2/\partial P)\,V = 0$.

Remark 5: The geometric indication of singularities resulting from S1 and S2 is that when actual velocity is a zero vector, or perpendicular to the tangent vector of the desired path, the controller is incapable of deciding which direction to turn the controlled vehicle.

To avoid singularities, a new speed error is introduced

$$\varepsilon_3 \triangleq \left(\frac{\partial f_1}{\partial P} \times \frac{\partial f_2}{\partial P}\right) V - \left\| \frac{\partial f_1}{\partial P} \times \frac{\partial f_2}{\partial P} \right\| v_r. \tag{22}$$

It follows from (18) and (22) that

$$[\ddot{\varepsilon}_1 \quad \ddot{\varepsilon}_2 \quad \dot{\varepsilon}_3]^T = \mathscr{H}(x, y, z, \dot{x}, \dot{y}, \dot{z}) + \mathscr{G}(x, y, z)\dot{V} \tag{23}$$

where

$$\mathscr{H} = [H_1, H_2, H_3]^T$$
$$\mathscr{G} = \left[G_1^T, G_2^T, \left(\frac{\partial f_1}{\partial P} \times \frac{\partial f_2}{\partial P}\right)^T \right]^T$$

and

$$H_3 = \left[\frac{\mathrm{d}}{\mathrm{d}t}\left(\frac{\partial f_1}{\partial P} \times \frac{\partial f_2}{\partial P}\right)\right] V - \left[\frac{\mathrm{d}}{\mathrm{d}t}\left\|\frac{\partial f_1}{\partial P} \times \frac{\partial f_2}{\partial P}\right\|\right] v_r - \left\|\frac{\partial f_1}{\partial P} \times \frac{\partial f_2}{\partial P}\right\| \dot{v}_r.$$

Therefore, $\det(\mathscr{G}) = \|\partial f_1/\partial P \times \partial f_2/\partial P\|^2 > 0$ holds locally around the reference path, and singularities resulting from S1 and S2 are avoided.

Remark 6: The first term at the right-hand side of (22) represents the projection of actual velocity onto the desired path, and the second term is always positive. Geometric implication of (22) is that the desired direction for velocity is assigned along the tangent vector of desired path.

Remark 7: Using the approach in Appendix B, it can be proved that if $\dot{\varepsilon}_1 = 0$, $\dot{\varepsilon}_2 = 0$, and $\varepsilon_3 = 0$, then $\|V\| = v_r$, suggesting that (22) does depict the speed error.

C. Command Filtered Backstepping Design

Step 1 (Virtual Control to Stabilize Path-Following Errors): Substituting (13) into (21) yields

$$\begin{aligned}[\ddot{\varepsilon}_1 \quad \ddot{\varepsilon}_2 \quad \dot{\varepsilon}_3]^T &= \mathscr{H} + \mathscr{G}\left(-g_3 + \frac{T_m}{m} R_3\right) \\ &= \mathscr{H} + \mathscr{G}\left(-g_3 + \frac{T_m}{m}\left[\bar{R}_3^T, \mathrm{c}\phi\mathrm{c}\theta\right]^T\right) \\ &= \mathscr{H} + \mathscr{G}\left(-g_3 + \frac{1}{m}\alpha_\varepsilon + \frac{T_m}{m}\left[(\bar{R}_{3e} + \tilde{\bar{\alpha}}_\varepsilon)^T, 0\right]^T\right)\end{aligned} \tag{24}$$

where the virtual control is defined by

$$\alpha_\varepsilon \triangleq T_m[\bar{\alpha}_\varepsilon^T, \mathrm{c}\phi\mathrm{c}\theta]^T \tag{25}$$

and $\bar{\alpha}_\varepsilon$ is the reference signal to be tracked by the attitude subsystem; command filtered reference signal is designed by

$$\hat{\bar{\alpha}}_\varepsilon(s) = \frac{\omega_n^2}{s^2 + 2\xi_n\omega_n + \omega_n^2}\bar{\alpha}_\varepsilon(s) \tag{26}$$

reference signal error and attitude tracking error are defined by $\tilde{\bar{\alpha}}_\varepsilon = \hat{\bar{\alpha}}_\varepsilon - \bar{\alpha}_\varepsilon$ and $\bar{R}_{3e} = \bar{R}_3 - \hat{\bar{\alpha}}_\varepsilon$, respectively. In (26), ξ_n and ω_n are command filter parameters.

Design the virtual control

$$\alpha_\varepsilon = m\left[g_3 + \mathscr{G}^{-1}(-\mathscr{H} + \mu_\varepsilon)\right] \tag{27}$$

with the stabilizing term given by

$$\mu_\varepsilon = -K_\varepsilon\varepsilon = \begin{bmatrix} -k_{11}\dot{\varepsilon}_1 - k_{12}\varepsilon_1 \\ -k_{21}\dot{\varepsilon}_2 - k_{22}\varepsilon_2 \\ -k_{31}\varepsilon_3 \end{bmatrix} \tag{28}$$

where $\varepsilon \triangleq [\varepsilon_1, \dot{\varepsilon}_1, \varepsilon_2, \dot{\varepsilon}_2, \varepsilon_3]^T$ is the error vector, K_ε is a 3×5 matrix, and $k_{ij} > 0$ are control parameters. Main rotor thrust can be calculated from (27)

$$T_m = \frac{e_3^T\alpha_\varepsilon}{\mathrm{c}\phi\mathrm{c}\theta}. \tag{29}$$

Substituting (27) and (28) into (24) yields

$$[\ddot{\varepsilon}_1 \quad \ddot{\varepsilon}_2 \quad \dot{\varepsilon}_3]^T = -K_\varepsilon\varepsilon + \frac{T_m}{m}\mathscr{G}\left[(\bar{R}_{3e} + \tilde{\bar{\alpha}}_\varepsilon)^T, 0\right]^T.$$

Set $L_1 = 1/2\varepsilon^T U\varepsilon$ as the Lyapunov candidate, where

$$U = \begin{bmatrix} U_1 & 0_{2\times 2} & 0_{2\times 1} \\ 0_{2\times 2} & U_2 & 0_{2\times 1} \\ 0_{1\times 2} & 0_{1\times 2} & u_3 \end{bmatrix}$$
$$U_i = \begin{bmatrix} \frac{1+k_{i2}}{k_{i1}} + \frac{k_{i1}}{k_{i2}} & \frac{1}{k_{i2}} \\ \frac{1}{k_{i2}} & \frac{1+k_{i2}}{k_{i1}k_{i2}} \end{bmatrix} \triangleq \begin{bmatrix} a & c \\ c & b \end{bmatrix}$$

and $u_3 = 1/k_{31} \triangleq d$. Eigenvalues of U_i are positive, showing that $L_1 > 0$. Its derivative can be calculated by

$$\dot{L}_1 = -\|\varepsilon\|^2 + \frac{T_m}{m}\bar{\varepsilon}^T\bar{G}\left(\bar{R}_{3e} + \tilde{\bar{\alpha}}_\varepsilon\right)$$

where $\bar{\varepsilon} = [c\varepsilon_1 + b\dot{\varepsilon}_1, c\varepsilon_2 + b\dot{\varepsilon}_2, d\varepsilon_3]^T$, and

$$\bar{G} = \begin{bmatrix} \frac{\partial f_1}{\partial x} & \frac{\partial f_1}{\partial y} \\ \frac{\partial f_2}{\partial x} & \frac{\partial f_2}{\partial y} \\ \frac{\partial f_1}{\partial y}\frac{\partial f_2}{\partial z} - \frac{\partial f_1}{\partial z}\frac{\partial f_2}{\partial y} & \frac{\partial f_1}{\partial z}\frac{\partial f_2}{\partial x} - \frac{\partial f_1}{\partial x}\frac{\partial f_2}{\partial z} \end{bmatrix}.$$

Step 2 (Virtual Control to Stabilize $\bar{R}_{3e}$): Reference signal for attitude kinematics is obtained by

$$\bar{\alpha}_\varepsilon = [e_1, e_2]^T\frac{\alpha_\varepsilon}{T_m} \tag{30}$$

where $e_1 \triangleq [1, 0, 0]^T$, $e_2 \triangleq [0, 1, 0]^T$, and $\bar{\alpha}_\varepsilon$ is to be tracked by the attitude subsystem.

Select the Lyapunov candidate $L_2 = c_\varepsilon L_1 + (1/2)\bar{R}_{3e}^T\bar{R}_{3e}$ with $c_\varepsilon > 0$. Its derivative can be calculated by

$$\begin{aligned}\dot{L}_2 &= c_\varepsilon\dot{L}_1 + \bar{R}_{3e}^T\dot{\bar{R}}_{3e} \\ &= c_\varepsilon\dot{L}_1 + \bar{R}_{3e}^T(\dot{\bar{R}}_3 - \dot{\hat{\bar{\alpha}}}_\varepsilon) \\ &= c_\varepsilon\dot{L}_1 + \bar{R}_{3e}^T(\hat{R}\bar{\omega} - \dot{\hat{\bar{\alpha}}}_\varepsilon) \\ &= c_\varepsilon\dot{L}_1 + \bar{R}_{3e}^T(\hat{R}\bar{\alpha}_R + \hat{R}\bar{\omega}_e + \hat{R}\tilde{\bar{\alpha}}_R - \dot{\hat{\bar{\alpha}}}_\varepsilon)\end{aligned}$$

where $\bar{\alpha}_R$ is the virtual control for stabilizing $\bar{R}_{3e}$; command filtered virtual control is designed by

$$\hat{\bar{\alpha}}_R(s) = \frac{\omega_n^2}{s^2 + 2\xi_n\omega_n + \omega_n^2}\bar{\alpha}_R(s) \tag{31}$$

command filtered and attitude tracking errors are defined by $\tilde{\bar{\alpha}}_R = \hat{\bar{\alpha}}_R - \bar{\alpha}_R$ and $\bar{\omega}_e = \bar{\omega} - \hat{\bar{\alpha}}_R$, respectively.

Design virtual control

$$\bar{\alpha}_R = \hat{R}^{-1}\left(-k_R\bar{R}_{3e} + \dot{\hat{\bar{\alpha}}}_\varepsilon - \frac{c_\varepsilon T_m}{m}\bar{G}^T\bar{\varepsilon}\right) \tag{32}$$

where $k_R > 0$ is the control parameter; invertibility of $\hat{R}$ can be proved by calculating $\det(\hat{R}) = R_{11}R_{22} - R_{12}R_{21} \neq 0$.

Derivative of L_2 can be calculated by

$$\dot{L}_2 = -c_\varepsilon\|\varepsilon\|^2 - k_R\left\|\bar{R}_{3e}\right\|^2 + \bar{R}_{3e}^T\hat{R}\left(\bar{\omega}_e + \tilde{\bar{\alpha}}_R\right) + \frac{c_\varepsilon T_m}{m}\bar{\varepsilon}^T\bar{G}\tilde{\bar{\alpha}}_\varepsilon.$$

Step 3 (Virtual Control for Yaw Angle): Reference yaw angle is designed by

$$\psi_r = \text{atan2}(v, u) \tag{33}$$

such that head of the helicopter is expected to point forward.

Consider the yaw angle kinematics given by (16), and define $\psi_e = \psi - \hat{\psi}_r$, where

$$\hat{\psi}_r(s) = \frac{\omega_n^2}{s^2 + 2\xi_n\omega_n + \omega_n^2}\psi_r(s). \tag{34}$$

Choose the Lyapunov candidate $L_3 = (1/2)\psi_e^2$. It follows that:

$$\begin{aligned}\dot{L}_3 &= \psi_e\left(\frac{\mathrm{s}\phi}{\mathrm{c}\theta}q + \frac{\mathrm{c}\phi}{\mathrm{c}\theta}r - \dot{\hat{\psi}}_r\right)\\ &= \psi_e\left(\frac{\mathrm{s}\phi}{\mathrm{c}\theta}q + \frac{\mathrm{c}\phi}{\mathrm{c}\theta}\alpha_\psi - \dot{\hat{\psi}}_r + \frac{\mathrm{c}\phi}{\mathrm{c}\theta}r_e + \frac{\mathrm{c}\phi}{\mathrm{c}\theta}\tilde{\alpha}_\psi\right)\end{aligned}$$

where $r_e \triangleq r - \hat{\alpha}_\psi$; α_ψ denotes the virtual control; command filtered error $\tilde{\alpha}_\psi \triangleq \hat{\alpha}_\psi - \alpha_\psi$; command filtered virtual control is designed by

$$\hat{\alpha}_\psi(s) = \frac{\omega_n^2}{s^2 + 2\xi_n\omega_n + \omega_n^2}\alpha_\psi(s). \tag{35}$$

Design the virtual control

$$\alpha_\psi = \frac{-\mathrm{s}\phi}{\mathrm{c}\phi}q - \frac{\mathrm{c}\theta}{\mathrm{c}\phi}\left(k_\psi\psi_e - \dot{\hat{\psi}}_r\right) \tag{36}$$

where $k_\psi > 0$ is the control parameter. Then

$$\dot{L}_3 = -k_\psi\psi_e^2 + \frac{\mathrm{c}\phi}{\mathrm{c}\theta}\psi_e\left(r_e + \tilde{\alpha}_\psi\right).$$

Step 4 (Control Torque): Define $\alpha_R = [\bar{\alpha}_R^T, \alpha_\psi]^T$, $\hat{\alpha}_R = [\hat{\bar{\alpha}}_R^T, \hat{\alpha}_\psi]^T$, and $\tilde{\alpha}_R = [\tilde{\bar{\alpha}}_R^T, \tilde{\alpha}_\psi]^T$. Define $\omega_e = [\bar{\omega}_e^T, r_e]^T = \omega - \hat{\alpha}_R$. Select the Lyapunov candidate $L_4 = L_2 + L_3 + 1/2\omega_e^T J\omega_e$. It follows that:

$$\dot{L}_4 = \dot{L}_2 + \dot{L}_3 + \omega_e^T J\dot{\omega}_e = \dot{L}_3 + \omega_e^T(-S(\omega)J\omega + Q - J\dot{\hat{\alpha}}_R).$$

Design the control torque

$$Q = S(\omega)J\omega + J\dot{\hat{\alpha}}_R - k_\omega\omega_e - G_\gamma\bar{\gamma}_e \tag{37}$$

where $k_\omega > 0$ is the control parameter, and

$$G_\gamma = \begin{bmatrix}\hat{R} & 0_{2\times1}\\ 0_{1\times2} & \frac{c\phi}{c\theta}\end{bmatrix}, \quad \bar{\gamma}_e = \begin{bmatrix}\bar{R}_{3e}^T\\ \psi_e\end{bmatrix}.$$

The derivative of Lyapunov candidate can be calculated by

$$\begin{aligned}\dot{L}_4 = &-c_\varepsilon\|\varepsilon\|^2 - k_R\left\|\bar{R}_{3e}\right\|^2 - k_\psi\psi_e^2 - k_\omega\|\omega_e\|^2\\ &+\frac{c_\varepsilon T_m}{m}\bar{\varepsilon}^T\bar{G}\tilde{\bar{\alpha}}_\varepsilon + \bar{\gamma}_e^T G_\gamma\tilde{\alpha}_R.\end{aligned} \tag{38}$$

D. Calculating the Actual Controls

In the previous sections, control thrust T_m and torque Q are solved by (29) and (37). Actual controls θ_m, θ_t, a_s, and b_s can be calculated from thrust and torque through following steps.

θ_m can be obtained from (29)

$$t_{cm} = \frac{T_m}{\rho s_m A_m\Omega_m^2 R_m^2}, \quad \theta_m = \frac{3}{2}\left[\sqrt{\frac{s_m t_{cm}}{2}} + \frac{4t_{cm}}{a_m}\right] \tag{39}$$

and Q_m is determined by

$$q_{cm} = \frac{\delta}{8} + 1.13t_{cm}^{\frac{3}{2}}\sqrt{\frac{s_m}{2}}, \quad Q_m = q_{cm}\rho s_m A_m\Omega_m^2 R_m^3.$$

Then, $\tau = [T_t, a_s, b_s]^T$ can be obtained from (17)

$$\tau = Q_A^{-1}(Q - Q_B). \tag{40}$$

In (40), invertibility of Q_A can be proved by

$$\begin{aligned}\det(Q_A) = &\, l_t Q_m^2 + (h_m l_t - h_t l_m)h_m T_m^2\\ &+T_m h_m\left(L_b l_t + M_a(l_t - h_t)\right)\end{aligned}$$

where $T_m > 0$, $h_m \gg l_m$, and $l_t \gg h_t$, according to physical structures of typical helicopters.

In addition, the collective pitch of the tail rotor is yielded by

$$t_{ct} = \frac{T_t}{\rho s_t A_t\Omega_t^2 R_t^2}, \quad \theta_t = \frac{3}{2}\left[\sqrt{\frac{s_t t_{ct}}{2}} + \frac{4t_{ct}}{a_t}\right]. \tag{41}$$

E. Brief Summary of Control Algorithm

The path-following control algorithm designed in this brief can be summarized in the following steps.

1) Path-following errors are defined by (18) and (23).
2) Virtual control for stabilizing path-following errors are calculated by (27).
3) Main rotor thrust is obtained by (29), and reference signal for attitude is calculated by (30). Command filtered reference signal for attitude is calculated by (26). Virtual control for attitude is calculated by (32).
4) Reference yaw angle is given by (33); its command filtered signal is calculated by (34). Virtual control for yaw is designed by (36).
5) Control torque is designed by (37), where command filtered signal is given by (31) and (35).
6) Actual controls are obtained through (39)–(41).

F. Analysis on Closed-Loop System

In Section III-A, forces and torques are simplified such that the helicopter model appears cascaded. Small neglected terms (or small parasitic terms [14]) of forces and torques can be denoted by Δ_F and Δ_Q, which are often discarded [17], [20], or regarded as bounded disturbances [18], [19], because of physical restrictions of typical helicopters.

Assumption 2: Small parasitic terms satisfy $\|\Delta_F\| < \bar{\Delta}_F$ and $\|\Delta_Q\| < \bar{\Delta}_Q$, where $\bar{\Delta}_F$ and $\bar{\Delta}_Q$ are small positive numbers.

Proposition 1: Consider the model-scaled helicopter described by (1)–(4), with forces and torques given by (5) and (6). Suppose Assumption 1 and 2 are satisfied. Path-following errors are defined by (18) and (22). If the controller is designed according to algorithm presented in Section III-E, then: 1) path-following errors are locally ultimately bounded with tunable ultimate bounds and 2) the actual speed $\|V\| \approx v_r$.

Proof: Please see Appendix. ■

Remark 8: It seems that Assumption 2 is strong, because small parasitic terms Δ_F and Δ_Q are related to system states,

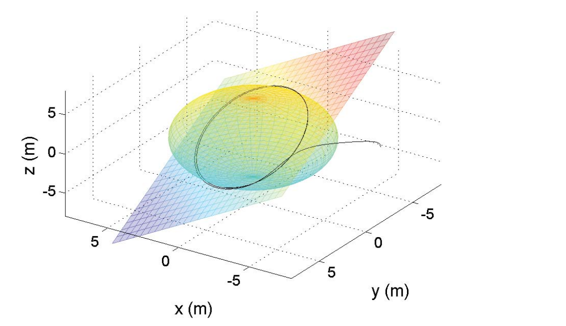

Fig. 2. 3-D illustration of path-following: the reference path is given by intersecting $x^2+y^2+z^2-25=0$ and $x+y+z=0$. Actual position of the helicopter is shown by the black solid curve.

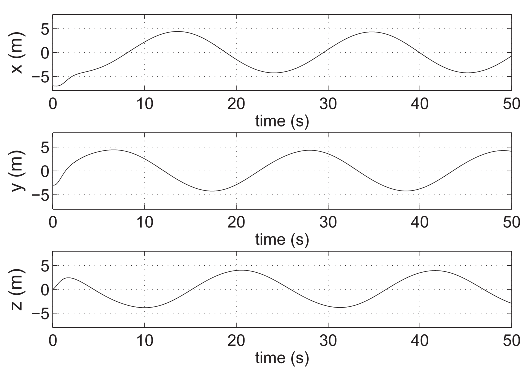

Fig. 3. Actual position of the controlled helicopter.

and boundedness of them requires predefined boundedness of system states. This issue would be addressed in future research. Practically, Δ_F and Δ_Q are usually extremely small according to physical restrictions of typical helicopters, such as mechanical restrictions of flapping angles and stiffness of rotor blades. Moreover, selecting appropriate control parameters would reduce the bounds of Δ_F and Δ_Q.

IV. Simulation and Discussion

A simulation example is given to illustrate the path-following controller. The reference path is a circular curve

$$\begin{cases} f_1(x_r, y_r, z_r) = x_r^2 + y_r^2 + z_r^2 - 25 \\ f_2(x_r, y_r, z_r) = x_r + y_r + z_r \end{cases} \tag{42}$$

which is the intersection of a plane and a ball. The reference speed is given by $v_r = 1.5$ (m/s). The complete model introduced in Section II-B is employed as the controlled plant. Values of aerodynamic parameters are cited from [21].

Applying the control algorithm stated in Section III-E, we can calculate that

$$\mathscr{H} = \begin{bmatrix} 2u^2 + 2v^2 + 2w^2 \\ 0 \\ -2v_r \cdot \frac{u(2x-y-z)+v(2y-z-x)+w(2z-x-y)}{\sqrt{(y-z)^2+(z-x)^2+(x-y)^2}} \end{bmatrix}$$

$$\mathscr{G} = \begin{bmatrix} 2x & 2y & 2z \\ 1 & 1 & 1 \\ 2(y-z) & 2(z-x) & 2(x-y) \end{bmatrix}.$$

Initial position $P(0) = [-7, -3, 0]^T$ (m) and initial yaw angle $\psi(0) = 1$(rad). The control algorithm is summarized in Section III-E, and the values of control parameters are listed in Table I. The simulation results are shown in Figs. 2–4.

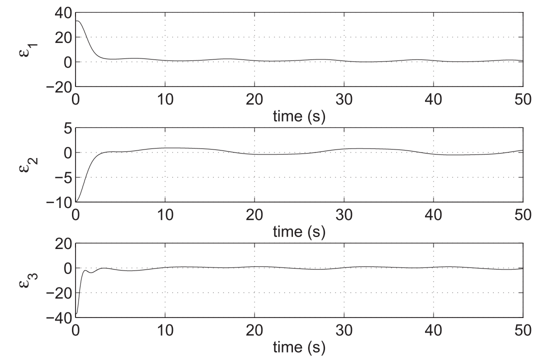

Fig. 4. Ultimately bounded path-following errors.

TABLE I
CONTROL PARAMETERS

$k_{11} = k_{21} = 1.5,\ k_{12} = k_{22} = k_{31} = 1,\ k_R = 4,$ $k_\psi = 0.5,\ k_\omega = 16,\ \xi_n = 0.707,\ \omega_n = 16$

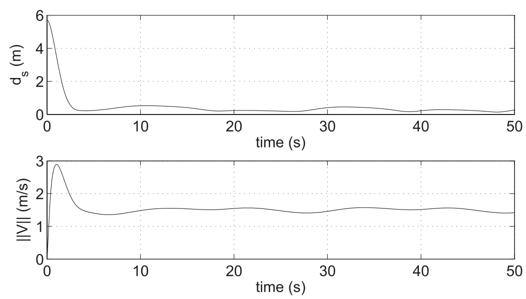

Fig. 5. Top: spatial distance from the helicopter to the reference path. Bottom: actual speed of the helicopter, approximately 1.5 (m/s).

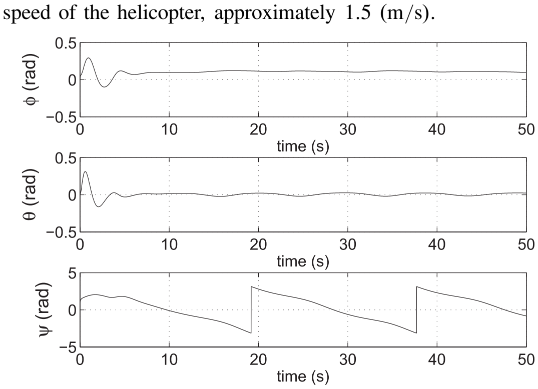

Fig. 6. Attitude of the fuselage during path-following: roll and pitch are fairly small, showing that the helicopter flies securely.

As shown in Figs. 2 and 3, the closed-loop system is capable to follow the reference path with bounded errors. No singularities occur during simulation. Fig. 4 shows that the path-following errors are bounded, as expected by Proposition 1. Ultimate bounds of the errors are fairly small, showing that side effects resulted from the small parasitic terms Δ_F and Δ_Q are negligible. Define the spatial distance from the controlled vehicle to the reference path by $d_s = \min \|P - P_r\||_{P_r \in \mathscr{P}_r}$. The spatial distance is shown in Fig. 5, which shows an intuitive explanation for physical meanings of the path-following. Also shown in Fig. 5, actual speed approaches the value of 1.5 (m/s). Roll and pitch angles are maintained in acceptable ranges, as shown in Fig. 6. Jumps from π to $-\pi$ in Fig. 6

show that the measurement range of yaw is $(-\pi, \pi]$, and actual values of yaw are added by $\pm 2k\pi$ until they enter the range. The simulation results demonstrate that the proposed path-following controller is capable to complete the predefined path-following task.

It should be noted that theoretical results in this brief are local, and only singularities resulted from S1 and S2 are avoided. We acknowledge that, if the initial position is located excessively far from the reference path, the closed-loop system would confront singularities resulted from $\|\partial f_1/\partial P \times \partial f_2/\partial P\| = 0$.

V. Conclusion

In this brief, a novel 3-D path-following controller is proposed for a 6-DOF model-scaled helicopter. The reference path to be followed is described by implicit expressions. Main theoretical results include the strategy of singularity avoidance and the application of command filtered backstepping. Both theoretical proof and simulation example demonstrate that, with the proposed controller, the path-following errors of the closed-loop system are locally ultimately bounded, while local singularities are avoided.

Some future works of this research include: 1) extending the proposed path-following controller to global cases by researching into geometric properties of reference paths and 2) relaxing Assumption 2 by considering detailed effects of parasitic terms.

Appendix A
Proof for Boundedness of Path-Following Errors

Consider the small neglected terms Δ_F and Δ_Q. The closed-loop system is now given by

$$[\ddot{\varepsilon}_1, \ddot{\varepsilon}_2, \dot{\varepsilon}_3]^T = -K_\varepsilon \varepsilon + \frac{T_m}{m}\mathscr{G}[(\bar{R}_{3e} + \tilde{\bar{\alpha}}_\varepsilon)^T, 0]^T + \Delta_F \quad (43)$$

$$\dot{\bar{R}}_{3e} = -k_R \bar{R}_{3e} + \hat{R}\bar{\omega}_e + \hat{R}\tilde{\bar{\alpha}}_R - \frac{c_\omega T_m}{m}\bar{G}^T\bar{\varepsilon} \quad (44)$$

$$\dot{\psi}_e = -k_\psi \psi_e + \frac{\mathrm{c}\phi}{\mathrm{c}\theta} r_e + \frac{\mathrm{c}\phi}{\mathrm{c}\theta}\tilde{\alpha}_\psi \quad (45)$$

$$J\dot{\omega}_e = -k_\omega \omega_e - G_\gamma \bar{\gamma}_e + \Delta_Q. \quad (46)$$

It follows from the theory of command filtered backstepping [12] that, corresponding with (43)–(46), a compensating system can be constructed

$$[\ddot{\xi}_{\varepsilon 1}, \ddot{\xi}_{\varepsilon 2}, \dot{\xi}_{\varepsilon 3}]^T = -K_\varepsilon \xi_\varepsilon + \frac{T_m}{m}\mathscr{G}\left[\left(\tilde{\bar{\alpha}}_\varepsilon + \bar{\xi}_R\right)^T, 0\right]^T \quad (47)$$

$$\dot{\bar{\xi}}_R = -k_R \bar{\xi}_R + \hat{R}\tilde{\bar{\alpha}}_R + \hat{R}\bar{\xi}_\omega - \frac{c_\omega T_m}{m}\bar{G}^T\bar{\xi}_\varepsilon \quad (48)$$

$$\dot{\xi}_\psi = -k_\psi \bar{\xi}_\psi + \frac{\mathrm{c}\phi}{\mathrm{c}\theta}\tilde{\alpha}_\psi + \frac{\mathrm{c}\phi}{\mathrm{c}\theta}\xi_r \quad (49)$$

where

$$\begin{aligned} \xi_\varepsilon &\triangleq [\xi_{\varepsilon 1}, \dot{\xi}_{\varepsilon 1}, \xi_{\varepsilon 2}, \dot{\xi}_{\varepsilon 2}, \xi_{\varepsilon 3}]^T \in \mathbb{R}^5 \\ \bar{\xi}_\varepsilon &= [c\xi_{\varepsilon 1} + b\dot{\xi}_{\varepsilon 1}, c\xi_{\varepsilon 2} + b\dot{\xi}_{\varepsilon 2}, d\xi_{\varepsilon 3}]^T \\ \xi_\gamma &\triangleq [\bar{\xi}_R^T, \xi_\psi]^T \in \mathbb{R}^3, \quad \bar{\xi}_R \in \mathbb{R}^2 \\ \bar{\xi}_\omega &= [0, 0]^T, \quad \xi_r = 0. \end{aligned}$$

Initial values of ξ_ε and $\bar{\xi}_R$ are all zeros.

Lemma 1: There always exists ω_n for command filters (26), (31), and (35), such that states of (47)–(49) are ultimately bounded with tunable ultimate bounds.

Proof: For command filters, given $\xi_n > 0$, $T > 0$, $\sigma_\varepsilon > 0$, $\sigma_R > 0$, and $\sigma_\psi > 0$, there always exists $\omega_n(T, \sigma_\varepsilon, \sigma_R, \sigma_\psi) > 0$, such that, when $t > T$

$$\begin{aligned} \|\tilde{\bar{\alpha}}_\varepsilon(t)\| &< \left\| \frac{m}{T_m}\mathscr{G}^{-1} \right\| \sigma_\varepsilon \\ \|\tilde{\bar{\alpha}}_R(t)\| &< \|\hat{R}^{-1}\|\sigma_R \\ \|\tilde{\alpha}_\psi(t)\| &< \frac{\mathrm{c}\theta}{\mathrm{c}\phi}\sigma_\psi. \end{aligned}$$

Select Lyapunov candidate $L_\xi = c_\varepsilon/2\xi_\varepsilon^T U\xi_\varepsilon + 1/2\bar{\xi}_R^T\bar{\xi}_R + 1/2\xi_\psi^2$. It follows that: $a_\xi\|\xi_\delta\|^2 \leqslant L_\xi \leqslant b_\xi\|\xi_\delta\|^2$, where $a_\xi \triangleq \min(c_\varepsilon/2\|U\|, 1/2)$, $b_\xi \triangleq \max(c_\varepsilon/2\|U\|, 1/2)$, and $\xi_\delta \triangleq \left[\|\xi_\varepsilon\|, \|\xi_\gamma\|\right]^T$. When $t > T$

$$\begin{aligned} \dot{L}_\xi &\leqslant -c_\varepsilon\|\xi_\varepsilon\|^2 - k_R\|\bar{\xi}_R\|^2 - k_\psi\|\xi_\psi\|^2 + \bar{\xi}_\varepsilon^T\sigma_\varepsilon + \bar{\xi}_R^T\sigma_R + \xi_\psi\sigma_\psi \\ &\leqslant -(c_\varepsilon - \theta_\varepsilon)\|\xi_\varepsilon\|^2 - (k_R - \theta_R)\|\bar{\xi}_R\|^2 - (k_\psi - \theta_\psi)\|\xi_\psi\|^2 \\ &\quad -\theta_\varepsilon\|\xi_\varepsilon\|^2 - \theta_R\|\bar{\xi}_R\|^2 - \theta_\psi\|\xi_\psi\|^2 + \bar{\xi}_\varepsilon^T\sigma_\varepsilon + \bar{\xi}_R^T\sigma_R + \xi_\psi\sigma_\psi \\ &\leqslant -(c_\varepsilon - \theta_\varepsilon)\|\xi_\varepsilon\|^2 - (k_R - \theta_R)\|\bar{\xi}_R\|^2 - (k_\psi - \theta_\psi)\|\xi_\psi\|^2 \\ &\quad + \frac{\sigma_\varepsilon^2}{4\theta_\varepsilon} + \frac{\sigma_R^2}{4\theta_R} + \frac{\sigma_\psi^2}{4\theta_\psi} \\ &\leqslant -c_\xi\|\xi_\delta\|^2 + d_\xi \end{aligned}$$

where $c_\xi \triangleq \min(c_\varepsilon - \theta_\varepsilon, k_R - \theta_R, k_\psi - \theta_\psi)$, $d_\xi \triangleq \sigma_\varepsilon^2/4\theta_\varepsilon + \sigma_R^2/4\theta_R + \sigma_\psi^2/4\theta_\psi$, $0 < \theta_\varepsilon < c_\varepsilon$, $0 < \theta_R < k_R$, and $0 < \theta_\psi < k_\psi$.

The Lyapunov candidate and its derivative show that the states of (47)–(49) are ultimately bounded

$$\|\xi_\delta\| \leqslant \sqrt{\frac{1}{a_\xi}\left(L_\xi(T) - \frac{b_\xi d_\xi}{c_\xi}\right)e^{-\frac{c_\xi}{b_\xi}(t-T)} + \frac{b_\xi d_\xi}{a_\xi c_\xi}}. \quad (50)$$

Ultimate bounds can be tuned by c_ξ, which is calculated from control parameters. ■

Define compensated tracking errors

$$\begin{aligned} \nu_\varepsilon &\triangleq \varepsilon - \xi_\varepsilon, \quad \bar{\nu}_R \triangleq \bar{R}_{3e} - \bar{\xi}_R \\ \nu_\psi &\triangleq \psi_e - \xi_\psi, \quad \nu_\omega \triangleq \omega_e - \xi_\omega \end{aligned}$$

where $\xi_\omega = [\bar{\xi}_\omega^T, \xi_r]^T$. It follows that:

$$[\ddot{\nu}_{\varepsilon 1}, \ddot{\nu}_{\varepsilon 2}, \dot{\nu}_{\varepsilon 3}]^T = -K_\varepsilon \nu_\varepsilon + \frac{T_m}{m}\mathscr{G}[\bar{\nu}_R^T, 0]^T + \Delta_F \quad (51)$$

$$\dot{\bar{\nu}}_R = -k_R\bar{\nu}_R + \hat{R}\bar{\nu}_\omega - \frac{c_\omega T_m}{m}\bar{G}^T\bar{\nu}_\varepsilon \quad (52)$$

$$\dot{\nu}_\psi = -k_\psi\nu_\psi + \frac{\mathrm{c}\phi}{\mathrm{c}\theta}\nu_r \quad (53)$$

$$J\dot{\nu}_\omega = -k_\omega\nu_\omega - G_\gamma\nu_\gamma + \Delta_Q \quad (54)$$

where $\bar{\nu}_\omega \triangleq \bar{\omega}_e - \bar{\xi}_\omega$ and $\nu_\gamma \triangleq [\bar{\nu}_R^T, \nu_\psi]^T$.

Lemma 2: States of (51)–(54) are ultimately bounded with tunable ultimate bounds.

Proof: Select the Lyapunov candidate

$$L_\nu = \frac{c_\varepsilon}{2}\nu_\varepsilon^T U\nu_\varepsilon + \frac{1}{2}\bar{\nu}_R^T\bar{\nu}_R + \frac{1}{2}\nu_\psi^2 + \frac{1}{2}\nu_\omega^T J\nu_\omega. \quad (55)$$

It follows that: $a_\nu \|\nu_\delta\|^2 \leqslant L_\nu \leqslant b_\nu \|\nu_\delta\|^2$, where

$$a_\nu \triangleq \min\left(\frac{c_\varepsilon}{2}\|U\|, \frac{1}{2}, \frac{1}{2}\|J\|\right) \tag{56}$$

$$b_\nu \triangleq \max\left(\frac{c_\varepsilon}{2}\|U\|, \frac{1}{2}, \frac{1}{2}\|J\|\right) \tag{57}$$

$$\nu_\delta \triangleq \left[\|\nu_\varepsilon\|, \|\nu_\gamma\|, \|\nu_\omega\|\right]^T. \tag{58}$$

Derivative of Lyapunov candidate can be calculated by

$$\begin{aligned}\dot{L}_\nu &= -c_\varepsilon\|\nu_\varepsilon\|^2 - k_R\|\bar{\nu}_R\|^2 - k_\psi\|\nu_\psi\|^2 - k_\omega\|\nu_\omega\|^2 \\ &\quad +\bar{\nu}_\varepsilon^T\Delta_F + \nu_\omega^T\Delta_Q \\ &\leqslant -(c_\varepsilon - \theta_\varepsilon)\|\nu_\varepsilon\|^2 - k_\gamma\|\nu_\gamma\|^2 - (k_\omega - \theta_\omega)\|\nu_\omega\|^2 \\ &\quad -\theta_\varepsilon\|\nu_\varepsilon\|^2 - \theta_\omega\|\nu_\omega\|^2 + \bar{\Delta}_F\|\nu_\varepsilon\| + \bar{\Delta}_Q\|\nu_\omega\| \\ &\leqslant -(c_\varepsilon - \theta_\varepsilon)\|\nu_\varepsilon\|^2 - k_\gamma\|\nu_\gamma\|^2 - (k_\omega - \theta_\omega)\|\nu_\omega\|^2 \\ &\quad +\frac{\bar{\Delta}_F^2}{4\theta_\varepsilon} + \frac{\bar{\Delta}_Q^2}{4\theta_\omega} \\ &\leqslant -c_\nu\|\nu_\delta\|^2 + d_\nu \end{aligned} \tag{59}$$

where $k_\gamma \triangleq \min\left(k_R, k_\psi\right)$, $c_\nu \triangleq \min\left(c_\varepsilon - \theta_\varepsilon,\ k_\gamma,\ k_\omega - \theta_\omega\right)$, $d_\nu \triangleq \bar{\Delta}_F^2/4\theta_\varepsilon + \bar{\Delta}_Q^2/4\theta_\omega$, $0 < \theta_\varepsilon < c_\varepsilon$, and $0 < \theta_\omega < k_\omega$. Equations (55) and (59) show that ν_δ is ultimately bounded

$$\|\nu_\delta\| \leqslant \sqrt{\frac{1}{a_\nu}\left(L_\nu(0) - \frac{b_\nu d_\nu}{c_\nu}\right)e^{-\frac{c_\nu}{b_\nu}t} + \frac{b_\nu d_\nu}{a_\nu c_\nu}}. \tag{60}$$

Ultimate bounds can be tuned by c_ν, which is calculated from control parameters. ■

Define $\delta \triangleq \left[\|\varepsilon\|, \|\bar{R}_{3e}\|, \|\psi_e\|, \|\omega_e\|\right]^T$. It is obvious that $\|\delta\| \leqslant \|\xi_\delta\| + \|\nu_\delta\|$. Results of Lemmas 1 and 2 imply that δ is ultimately bounded with tunable ultimate bounds; therefore, the path-following errors are ultimately bounded.

The stability result of the closed-loop system is local, since the strategy of singularity avoidance is effective locally. If initial position is located excessively far from the reference path, the controlled helicopter would encounter singularities.

Remark 9: It seems from (50) and (60) that ultimate bounds can be tuned arbitrarily small by setting large enough control parameters; however, excessively large control parameters would result in aggressive velocity or attitude, destroying Assumptions 1 and 2.

APPENDIX B
PROOF FOR PERFORMANCE OF ACTUAL SPEED

It is proved in Appendix A that, after some setting time, ε_3 is ultimately bounded within small ultimate bounds, showing

$$\left(\frac{\partial f_1}{\partial P} \times \frac{\partial f_2}{\partial P}\right)V \approx \left\|\frac{\partial f_1}{\partial P} \times \frac{\partial f_2}{\partial P}\right\| v_r > 0. \tag{61}$$

Errors ε_1, $\dot{\varepsilon}_1$, ε_2, and $\dot{\varepsilon}_2$ are stabilized within small neighborhoods of zero. It follows from (19) that $(\partial f_1/\partial P)V \approx 0$ and $(\partial f_2/\partial P)V \approx 0$, suggesting that V is approximately perpendicular with both $(\partial f_1/\partial P)^T$ and $(\partial f_2/\partial P)^T$, thus parallel with $(\partial f_1/\partial P \times \partial f_2/\partial P)^T$. Therefore, with its positiveness shown by (61)

$$\left(\frac{\partial f_1}{\partial P} \times \frac{\partial f_2}{\partial P}\right)V \approx \left\|\frac{\partial f_1}{\partial P} \times \frac{\partial f_2}{\partial P}\right\| \|V\|. \tag{62}$$

Considering (61), (62), and Remark 1, we conclude that $\|V\| \approx v_r$, which fulfills the requirement on velocity.

ACKNOWLEDGMENT

The authors would like to thank the reviewers for their insightful comments and creative suggestions.

REFERENCES

[1] A. P. Aguiar, J. P. Hespanha, and P. V. Kokotovic, "Performance limitations in reference tracking and path following for nonlinear systems," *Automatica*, vol. 44, no. 3, pp. 598–610, 2008.

[2] D. B. Dacic, D. Nesic, and P. V. Kokotovic, "Path following for nonlinear systems with unstable zero dynamic," *IEEE Trans. Autom. Control*, vol. 52, no. 3, pp. 481–487, Mar. 2007.

[3] D. B. Dacic, D. Nesic, A. R. Teel, and W. Wang, "Path following for nonlinear systems with unstable zero dynamic: An averaging solution," *IEEE Trans. Autom. Control*, vol. 56, no. 4, pp. 880–886, Apr. 2011.

[4] C. Altafini, "Path following with reduced off-tracking for multibody wheeled vehicles," *IEEE Trans. Control Syst. Technol.*, vol. 11, no. 4, pp. 598–605, Jul. 2003.

[5] L. Lapierre and D. Soetanto, "Nonlinear path following control of an AUV," *Ocean Eng.*, vol. 34, no. 11, pp. 1734–1744, 2007.

[6] I. Kaminer, A. Pascoal, E. Xargay, N. Hovakimyan, C. Cao, and V. Dobrokhodov, "Path following for unmanned aerial vehicle using L_1 adaptive augmentation of commercial autopilots," *AIAA J. Guid., Control Dyn.*, vol. 33, no. 2, pp. 550–564, 2010.

[7] V. Cichella, E. Xargay, V. Dobrokhodov, I. Kaminer, A. Pascoal, and N. Hovakimyan, "Geometric 3D path following control for a fixed-wing UAV on SO_3," in *Proc. AIAA Guid., Navigat., Control Conf.*, Aug. 2011, pp. 1–15.

[8] P. Liljeback, I. U. Haugstuen, and K. Y. Pettersen, "Path following control of planar snake robots using a cascaded approach," *IEEE Trans. Control Syst. Technol.*, vol. 20, no. 1, pp. 111–126, Jan. 2011.

[9] A. P. Aguiar and J. P. Hespanha, "Trajectory-tracking and path following of underactuated autonomous vehicles with parametrc modeling uncertainty," *IEEE Trans. Autom. Control*, vol. 52, no. 8, pp. 1362–1379, Aug. 2007.

[10] C. Nielsen, C. Fulford, and M. Maggiore, "Path following using transverse feedback linearization: Application to a maglev positioning system," *Automatica*, vol. 46, no. 3, pp. 585–590, 2010.

[11] J. A. Farrell, M. Polycarpou, M. Sharma, and W. Dong, "Command filtered backstepping," *IEEE Trans. Autom. Control*, vol. 54, no. 6, pp. 1391–1395, Jun. 2009.

[12] W. Dong, J. A. Farrell, M. Polycarpou, V. Djapic, and M. Sharma, "Command filtered adaptive backstepping," *IEEE Trans. Control Syst. Techol.*, vol. 20, no. 3, pp. 566–580, May 2012.

[13] B. Zhu and W. Huo, "Adaptive backstepping control for a miniature autonomous helicopter," in *Proc. 50th IEEE CDC-ECC*, Dec. 2011, pp. 5413–5418.

[14] I. A. Raptis, K. P. Valavanis, and W. A. Moreno, "A novel nonlinear backstepping controller design for helicopters using the rotation matrix," *IEEE Trans. Control Syst. Tech.*, vol. 19, no. 2, pp. 465–473, Mar. 2011.

[15] T. J. Koo and S. Sastry, "Output tracking control design of a helicopter model based on approximate linearization," in *Proc. 37th IEEE CDC*, Dec. 1998, pp. 3635–3640.

[16] A. R. S. Bramwell, G. Done, and D. Balmford, *Bramwell's Helicopter Dynamics*, 2nd ed. Oxford, U.K.: Butterworth Heinmann, 2001, pp. 48–51.

[17] A. Isidori, L. Marconi, and A. Serrani, "Robust nonlinear motion control of a helicopter," *IEEE Trans. Autom. Control*, vol. 48, no. 3, pp. 413–426, Mar. 2003.

[18] O. Shakernia, Y. Ma, T. J. Koo, and S. Sastry, "Landing an unmanned air vehicle: Vision Based motion estimation and nonlinear control," *Asian J. Control*, vol. 1, no. 3, pp. 128–145, Sep. 1999.

[19] I. A. Raptis, K. P. Valavanis, and G. J. Vachtsevanos, "Linear tracking control for small-scale unmanned helicopters," *IEEE Trans. Control Syst. Technol.*, vol. 20, no. 4, pp. 995–1010, Jul. 2012.

[20] L. Marconi and R. Naldi, "Robust full degree-of-freedom tracking control of a helicopter," *Automatica*, vol. 43, no. 11, pp. 1909–1920, 2007.

[21] V. Gavrilets, "Autonomous aerobatic maneuvering of miniature helicopter," Ph.D. dissertation, Dept. Aeronautics Astron., Massachusetts Inst. Technol., Cambridge, MA, USA, 2003.